

PAPER

Engineering the apparent quantum yield and emission rate of fluorophore molecules by coupling fluorophore dipoles with plasmon modes of gold using low frequency electric fields

To cite this article: K A S Lakshan and D Nawarathna 2024 J. Phys. D: Appl. Phys. 57 455401

Oling - Plasi

- <u>Plasmon-Enhanced Photocatalysis on TiO_p-Passivated Gallium Phosphide</u> Stephen B. Cronin

You may also like
- Nano-enhanced!

Anna Demming

- (Invited, Digital Presentation)
 Enhancement of Magnetic Dipole
 Transition of Molecules By Silicon
 Nanoparticle Nanoantenna
 Minoru Fujii and Hiroshi Sugimoto

View the article online for updates and enhancements.



Engineering the apparent quantum yield and emission rate of fluorophore molecules by coupling fluorophore dipoles with plasmon modes of gold using low frequency electric fields

K A S Lakshan^{1,4} and D Nawarathna^{1,2,3,*}

- ¹ Department of Electrical and Computer Engineering, North Dakota State University, Fargo, ND 58102, United States of America
- ² Biomedical Engineering Program, North Dakota State University, Fargo, ND 58102, United States of America

E-mail: dnawarat@odu.edu

Received 21 December 2023, revised 17 June 2024 Accepted for publication 29 July 2024 Published 14 August 2024



Abstract

Localized surface plasmons produced by gold and silver nanostructures have been utilized to enhance the intensity of fluorophore molecules. The issue with using nanostructure plasmons for fluorescence enhancement is their short-range nature (5–50 nm from the nanostructures), which limits accessibility to a few molecules. In addition, fluorophore dipoles needed to be aligned with the plasmon electric fields to maximize the fluorescence enhancement. To address these issues, we used low-frequency electric fields (<5 MHz) and commercially available nanorod and nanosphere samples and studied their effectiveness in enhancing the fluorescence of fluorophore-labeled short single-stranded DNA molecules (22 bases). We demonstrated that DNA molecules and nanorod particles can effectively be manipulated around the charging frequency of DNA molecules (~3 MHz). Nanorod particles enhanced the fluorescence emission rate by \sim 50-fold. When the 3 MHz electric field was introduced, the emission rate increased to over 700-fold. We also found that the introduction of a 3 MHz electric field aided the enhancement of the intrinsic quantum yield fluorophore molecules, which resulted in over a 1000-fold fluorescence enhancement. This enhancement was due to the very high electric produced by polarized DNA dipoles at 3 MHz, which resulted in a torque on fluorophore dipoles and subsequently aligning the fluorophore dipole axis with the plasmon electric field. At a fundamental level, our results demonstrate the role of the low-frequency electric field in the fluorophore-plasmon coupling. These findings can directly be applied to many fluorescence detection systems, including the development of biosensors.

Supplementary material for this article is available online

Keywords: low frequency electric fields, nanoparticles, interdigitated electrodes, fluorescence enhancement, metal-fluorophore-electric field interactions and surface plasmons

³ Current address: Department of Electrical and Computer Engineering, Old Dominion University, Norfolk, VA, 23 529.

Current address: Department of Physics, University of Ruhuna, Sri Lanka.

^{*} Author to whom any correspondence should be addressed.

1. Introduction

Biosensor devices have become a vital part of medical screening, diagnostics, and health monitoring. However, there are significant challenges to overcome before these sensors are effectively utilized in a wide range of medical applications such as early cancer detection. The optical detection methods, including fluorescence, localized surface plasmon resonance, and surface-enhanced Raman scattering have been utilized in sensor development for disease biomarker detection [1–3]. Fluorescence-based detection methods have been proven to be more effective than other methods used for detecting biomarkers, including circulating DNA, proteins, and microRNA. This is in part because the use of fluorescence provides a quantifiable signal that correlates with the biomarker levels in a sample [4, 5]. However, even with sophisticated fluorescence detection methods commonly used in sensing applications such as sequence-specific detection (such as molecular beacons), molecular structure-based detection (such as SYBR green), and bead-based microarrays, the accurate detection of low levels (<pM) has been shown to be difficult [5–7].

Studies have shown that the excitation light in the visible range can excite the plasmonic modes including localized surface plasmons, on gold or silver nanostructures and produce plasmonic hotspots [8]. These excited plasmons can interact with nearby fluorophore molecules and enhance the fluorophore emission. Briefly, enhanced electric field regions in the hotspots could potentially increase the emission rate of fluorophore and subsequently the fluorescence intensity of the stable fluorophore molecules located in the hotspots [8, 9]. In addition, the interaction of the surface plasmons of hotspots with the fluorophore dipoles could also enhance the intrinsic quantum yield (OY) of the fluorophore molecules [9, 10]. Enhancing QY has been shown to be more effective for low QY fluorophores because the increase in QY produces stabilization of the fluorophores and makes them less susceptible to photobleaching in addition to causing an increase in the signalto-background ratio [9-13]. Additionally, fluorophores located in the hotspots can experience negative effects caused by the plasmons in the hotspots. Moreover, fluorophores located very close (<5 nm) to nanostructures can potentially cause photo-bleaching of the fluorophore intensity by producing an increase in the non-radiative energy decay rate and subsequently, a decrease in the QY [9–13]. Fundamentally, these fluorescence enhancement mechanisms use the interactions of fluorophore dipoles with gold or silver plasmons, including localized surface plasmons and surface plasmon polaritons (SPPs) [9-14]. One of the critical requirements needed to satisfy these fluorescence enhancement mechanisms is the placement of the fluorophore with respect to the hotspots. Ideally, fluorophore molecules located within 5-50 nm from the hotspots can effectively interact with hotspots. Therefore, the applicability of these fluorescence enhancement mechanisms is limited to fluorophores located closer to the hotspots. In addition, the extent of these fluorophore enhancement mechanisms is highly dependent on the orientation of the fluorophore dipole axis with the plasmonic dipole electric field [9–13]. Unfortunately, it is currently difficult to optimize these interactions to maximize fluorescence intensity. This lack of optimization could create a significant issue when detecting extremely weak fluorescence intensities. To address these fundamental limitations, studies developed and utilized various nanostructures [15], nanomaterials [16], atomic force microscope probe tips to act as hotspot [17], plasmonic photonic crystals [18] and other methods [19-21]. For example, Song et al, have utilized dielectric spacers to precisely engineer the fluorophore distance and enhance the fluorescence intensity. Additionally, a quantum mechanical model was developed to further explain the experimental findings as well as to use in future hotspot design [21]. These studies provided deeper understanding of the utility of materials and structure in fluorescence enhancement. In this study, we studied the utility of low-frequency electric fields (<5 MHz) applied to interdigitated electrodes and commercially available gold nanoparticles and evaluated this process's effectiveness in the enhancement of fluorescence intensity. Low frequency electric fields have very limited utility in fluorescence enhancement experiments. To demonstrate the utility of low frequency electric fields, we conducted experiments using short fluorophore-labeled DNA molecules.

2. Results and discussion

2.1. Molecular concentration effects on electrodes using low-frequency electric fields and subsequent effects on fluorescence intensity

Interdigitated electrode arrays have been used to apply lowfrequency electric fields in many biomedical applications. Interdigitated electrodes including T-shaped interdigitated electrodes (TIEs) utilized in experiments [9, 22-25]. It was demonstrated earlier that TIEs, especially because of their Tshape, produce non-uniform electric fields and larger electric field gradients (∇E^2) [23]. These electric fields and their gradients can be used to produce larger dielectrophoretic (DEP) forces and alternating current (AC) electro-osmosis drag forces (EOF) on biomarker molecules needed for manipulating the electrodes [23, 26]. Figure 1(a) shows the bright field view of the electrode area, including contact pads for applying external potentials, and the insets show the bright field view of a section of TIEs and scanning electron microscope image of a single T-electrode. Figure 1(b) illustrates the calculated electric field values (magnitudes), and the maximum electric field value of 10⁶ V m⁻¹ was reported near the straight sections of the T-electrode. To concentrate molecules by the electric fields or moreover, the DEP force $\left(\frac{\alpha\nabla\left(E^2\right)}{2}\right)$ related electric field must produce higher energy on the molecules than the thermal energy of the molecules; roughly, the electric field should satisfy the equation, $^1/_2(\alpha E^2) > kT$, in which α (=9 × 10⁻³⁰ Cm² V⁻¹) is the polarizability of the DNA molecules, T is the temperature, and E is the electric field. For concentrating short DNA molecules (~22 bases long) used in experiments, we calculated the minimum

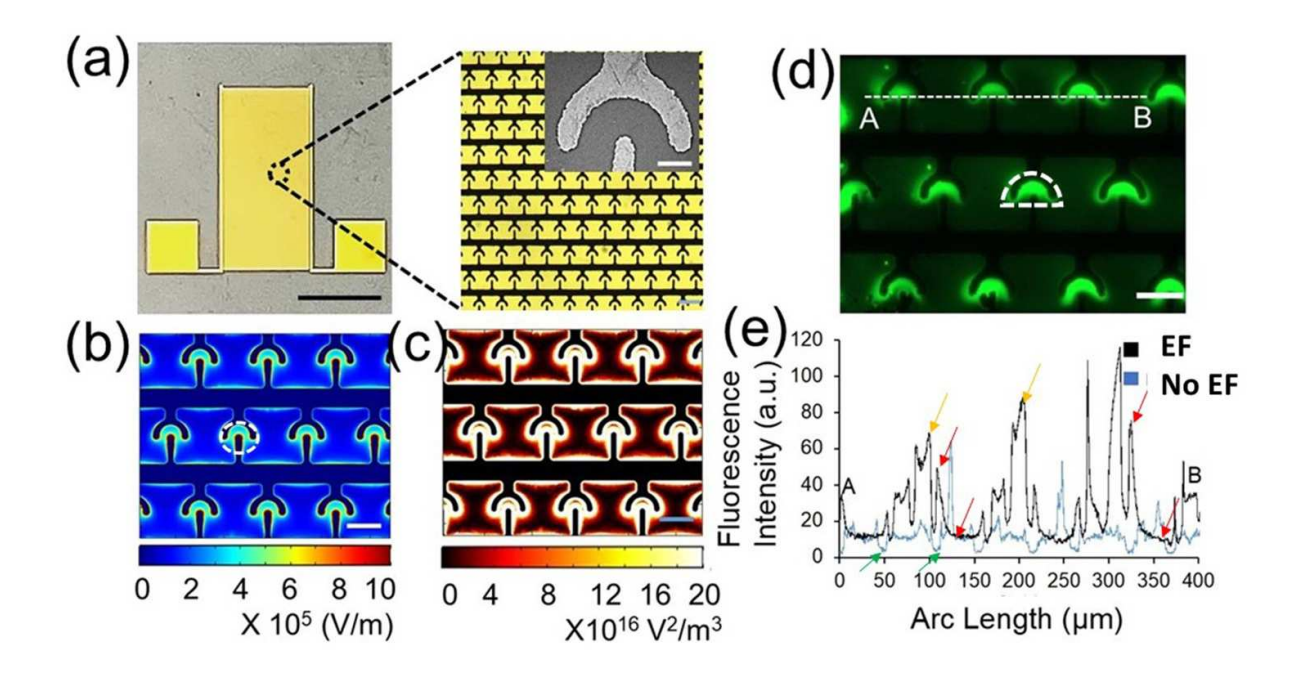


Figure 1

Figure 1. The device and the utility of low frequency electric fields for manipulation of fluorophore labeled DNA molecules. (a) A picture of a typical device used in experiments. Electric fields (10 Vpp at 0–5 MHz) were applied at the square pads. The long rectangular area shows the interdigitated T-electrodes (166 pairs). Scale bar shows 1 cm. Inset: bright field view of a section of interdigitated T-electrodes (scale bar 50 μ m). Scanning electron microscope image show a single 'T' electrode. Scale bar shows 10 μ m. (b) Calculated electric field distribution in the device for 10 Vpp applied voltage at the pads. (c) Calculated $\nabla (E^2)$ in the device for the applied voltage of 10 Vpp. (d) Typical image of the concentrated fluorophore labeled DNA molecules. 1 μ M fluorophore labeled molecules were used in the experiments and 10 Vpp (3 MHz) voltage was applied for about 10 mins. Scale bar illustrates 50 μ m. (e) Variation of the fluorescence intensity of the fluorophore labeled DNA along the contour A-B in (d) with and without electric fields (10 Vpp and 3 MHz).

electric field of $3.3 \times 10^4 \text{ V m}^{-1}$, which is needed to overcome the Brownian motion (due to thermal energy) and produce an electric field-driven motion [27, 28]. The circle with the broken line in figure 1(b) indicates the region in which molecules can experience motion due to the applied electric field. The approximate volume of the half-sphere is about 3 nl. We then calculated the magnitude of the electric field gradient on the electrode plane (figure 1(c)). The maximum value of the calculated electric field gradient value on the electrode plan was 10¹⁷ V² m⁻³, which could produce a nN DEP force on the 22-base DNA molecules. Figure 1(d) illustrates a fluorescence image of concentrated DNA molecules labeled with AF488 fluorophore molecules via the application of an electric field with 10 Vpp electric potential at 3 MHz. As expected, a significant accumulation of fluorescence was observed within the calculated volume around a T-electrode. To further understand the concentration of fluorophore-labeled DNA molecules on the T-electrodes using electric fields and DEP force, we have conducted additional experiments by varying the frequency of the applied electric field from 0 to 5 MHz (voltage = 10 Vpp) and calculated the fluorescence intensities at each frequency (figure 2). These experiments provide insight into the frequency-dependent polarization of fluorophore-labeled DNA molecules. The negative

control experiments were performed by pipetting the DNA molecules onto a microscope cover slide and measuring the fluorescence intensity. Additionally, we conducted experiments using AF488-, AF555-, and no fluorophore-labeled DNA and found that the maximum concentration occurred around 3 MHz for all molecules. This experimental result demonstrated that the major contribution to the DEP force of fluorophore-labeled DNA molecules is due to the polarization of DNA molecules, and the actual contribution from fluorophore molecules may be insignificant. The selection of the frequency range for the experiments is based on the charge relation time of the DNA molecules, which is the time required to build up the electric dipoles around the DNA molecules and polarize them. The charging time for short DNA molecules could be determined using the equation, $\tau =$ $\frac{L^2}{2D}$ in which L is the length of the DNA molecules, and \overrightarrow{D} is the diffusion coefficient [28]. Using 10^{-4} for the D, we calculated the relaxation time for the DNA molecules suspended in the low conductivity buffer $(0.001 \times TE)$ as \sim 4 μ s, which indicates that at least a 2.5 MHz frequency was needed to fully polarize the DNA molecules. Based on this calculation, we selected frequencies around 2.5 MHz (0-5 MHz) to study the variation of fluorescence intensity. When the applied frequency is >2.5 MHz, the

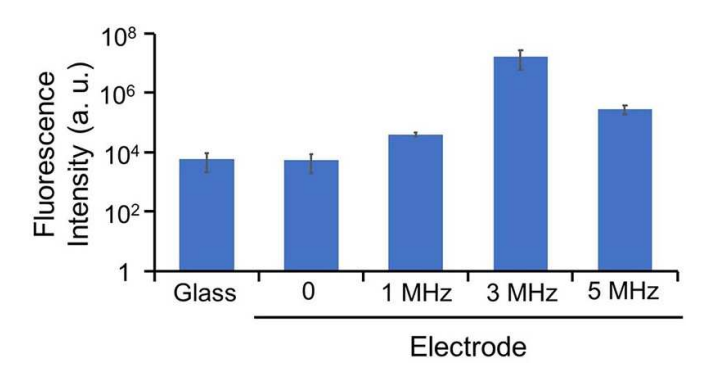


Figure 2. Variation of the fluorescence intensity of 1 μ M fluorophore labeled DNA (AF488) molecules in the device with the frequency of the applied electric field (10 Vpp). Increase in fluorescence intensity is due to the reduction of fluorophore quenching and increasing the emission rate of fluorophore molecules by the electric fields and DEP force of the fluorophore labeled DNA molecules.

polarizability of DNA molecules, more specifically, variation of frequency-dependent polarization, $\alpha(\omega) \propto \text{Re}\left(Q(\omega)\right)$ in which $Q(\omega)=Q_0\left[\frac{1}{1+(\omega au)^2}+j\frac{\omega au}{1+(\omega au)^2}
ight]$, and Q_0 is a constant. The $\alpha(\omega)$ value decreased after increasing the applied frequency [28]. Moreover, an approximately 50% decrease (between 2 and 5 MHz frequency) was expected. The decrease in fluorescence could have been due to the weakening polarizability and subsequently weak DEP force at higher frequencies (>2.5 MHz). If the applied frequency was <2.5 MHz, the polarizability of the DNA molecules would be strong, and subsequently, a strong DEP force on the DNA molecules was expected. Surprisingly, we observed a reduction in fluorescence at frequencies of <2.5 MHz. This reduction could have been due to the capacitance between the electrode and electrolyte interface called double-layer capacitance [29]. A voltage drop had been expected in the double layer and subsequently led to a decrease in the polarizability at the frequencies <2.5 MHz [29]. Since double-layer capacitance is inversely proportional to the frequency of the applied electric field, we expected a reduction in fluorescence at frequencies <2.5 MHz. For these reasons, we used 3 MHz in experiments to manipulate DNA molecules.

Although dielectrophoresis significantly contributes to the concentration of DNA molecules in T-electrodes, other processes, such as electrophoresis and Brownian motion, could also collectively contribute to the concentration of DNA molecules. For example, Brownian motion could contribute to the mixing of molecules outside the capture region and driving molecules toward the capture region. To further understand the dynamics of molecular concentration near the electrodes, we have analyzed the variation of the fluorescence intensity along a contour line across T-electrodes (see figure 1(e)). In general, the accumulation of DNA molecules at any point in the contour line is the result of an electric field (such as dielectrophoresis) and diffusion-dependent concentration of DNA molecules. We then used the modified Ficks's equation to

calculate the expected variation of the molecular concentration along the contour. At a thermodynamically steady state, the concentration of DNA molecules at any point can be represented using Boltzmann equation, and local DNA concentration could be written as $n(p,t) = n_0 e^{-\frac{\alpha E^2}{2kT}}$ in which n_0 is the DNA concentration at the highest gradient, t is the time, and p is the distance from the electrode to the observation point [28]. According to this analysis, an exponential decay function with the square of the local electric field dependent on the number of molecules would be expected. The region shown in red arrows in the contour produced with DEP force in figure 1(e) shows an exponential decay-like decrease in fluorescence intensity, which is consistent with the predicted behavior based on the Boltzmann equation.

A potential issue with the concentration of fluorophorelabeled DNA molecules in a smaller region is fluorophore quenching. When fluorophore-labeled molecules are concentrated, Förster resonance energy transfer (FRET) between fluorophore dipole molecules creates a reduction in the QY of the fluorophore molecules. The FRET rate is dependent on $\frac{1}{\sqrt{6}}$ in which d is the distance between fluorophore dipoles [30]. Generally, FRET is effective when d < 10 nm and takes place when target molecules (such as DNA) are labeled with multiple fluorophores [30, 31]. To study the concentrationdependent fluorophore quenching, we calculated the fluorescence intensity variation with different molecular concentrations of fluorophore-labeled DNA and found that fluorescence intensity has a linear relationship with the molarity of the molecules (see supplemental figure S1). If quenching had occurred, we would have expected a reduction in fluorescence intensity or a nonlinear relationship with concentration. Based on this analysis, it is unlikely that fluorophore quenching due to a concentration-dependent effect for AF488 molecules occurred.

Additionally, figure 1(e) illustrates the variation in fluorescence when the electric fields (DEP force) on DNA molecules are absent. In comparison, the fluorescence intensity measured by applying electric fields shows a significant increase in some regions such as near electrodes or regions shown in yellow color arrows in figure 1(e), and other regions (see green color arrows in figure 1(e)) show a decrease in fluorescence levels. As expected, the DEP force could facilitate a concentration of molecules in the high electric field gradient regions (∇E^2) , which would produce an accumulation of fluorescence intensity. Especially, the reduction in fluorescence intensity could be due to the photobleaching of fluorescence molecules caused by the gold electrodes. The excitation light produces surface plasmons on the gold electrodes, and fluorophore molecules harness energy from plasmons. However, when a fluorophore is located within about 5 nm of the gold electrodes, a significant portion of harnessed energy, called nonradiative energy, is lost or not available for fluorophore molecules [10, 32]. Non-radiative energy produces a decrease in the intrinsic QY of the fluorophore molecule and subsequently causes photobleaching of the fluorophore. Moreover, the nonradiative decay rate (γ_{nr}) of fluorophore molecule is inversely

proportional to the QY (η) of the fluorophore. For example, when a fluorophore is placed near a nanoparticle, $\gamma_{\rm nr} \propto \frac{1}{(r-a)^6}$ in which r is the distance to the center of the fluorophore dipole, a is the radius of the metal particle, and $\eta \to 0$ when $(r-a) \to 0$ [33]. Our experimental data agree with this prediction for the experiments without an applied electric field or no DEP force on the molecules. Surprisingly, no reduction in fluorescence intensity was observed when an electric field had been applied and produced a DEP force on the molecules. Moreover, under these experimental conditions, fluorescence intensity was increased near the electrodes. This means that the application of an electric field and subsequent DEP force yields the minimum amount of fluorophore quenching.

Broadly, low-frequency electric fields (e.g. 0-5 MHz) produce DEP force and EOF on the DNA molecules suspended in the low conductivity buffer that we used in the experiments. The EOF flow velocity is given by $v = \frac{DE_1\sigma}{\rho}$ in which D is the Debye length, ρ is the viscosity, σ is the surface charge density in the diffuse layer, and E_t is the tangential electric field [34]. We estimated that a maximum of about 8–10 μ m s⁻¹ velocity would be possible for the experimental conditions that we used in experiments. EOF produces viscous drag force on the DNA molecules, and as a result, at least two forces (drag and DEP forces) are exerted on the DNA molecules. In addition, electric fields can stretch the DNA molecules. Our experimental results show that the result of these two forces and DNA stretching collectively caused the transport of the fluorophore-labeled DNA molecules outside the quenching region. The length of the DNA, when it is fully stretched, is \sim 8–10 nm, and the EOF drag force and DEP force could potentially keep the fluorophore out of the quenching region (>5 nm). This process would only be possible when the fluorophore end (3' or 5') of the DNA was placed away from the metal electrodes. If the fluorophore end is concentrated next to the metal electrode, those fluorophore molecules would be quenched. Our data suggest that the former process is dominant. This scenario is possible when DNA has higher polarizability (strong DEP force) than the fluorophore molecule at 3 MHz. To further support this claim, we demonstrated earlier that electric fields applied at 3 MHz can be used to minimize the quenching of DNA molecules labeled with other fluorophore molecules [23]. We have further investigated other potential avenues to explain this experimental result, which will be discussed later in this study.

When comparing the fluorescence intensity levels with and without electric fields, a significant fluorescence concentration was observed to be very close to the T-electrode with electric fields (see figures 1(d) and (e)). Interestingly, the fluorescence intensity levels with and without an electric field outside the electrodes were almost identical (see figure 1(e)). This finding means that the capabilities of the electric fields to concentrate molecules are highly localized to the electrodes. Accurate counting of the molecules of interest within the entire sample pipetted on the electrodes is needed in some biomedical applications, including biosensing. AC

electro-osmosis, electrothermal mobility, thermophoresis, and diffusion methods have been used to concentrate molecules on the detection electrodes [23]. These methods, when compared with dielectrophoresis, are considered long-range effects that can reach the molecules located as far few centimeters from the electrodes [23]. However, the issue is the lack of selectivity toward the target molecules. In this work, we first used gold nanoparticles (spheres and rods) as delivery vehicles that can efficiently fetch biomolecules locally and transport them to electrodes and concentrate. In addition to spheres and rods. other nanoparticles have also been utilized in experiments. For example, Hai et al, have studied the in-situ growth of hotspots out of nano-composite materials for biosensing [35]. Additionally, in another study, water dispersible silver nanoparticles were prepared, characterized, and utilized in biosensor applications [36]. Second and finally, we investigated the use of low-frequency electric fields (<5 MHz) in terms of enhancing the fluorescence intensity of the fluorophorelabeled biomarkers molecules.

2.2. Interaction of gold nanoparticles, fluorophore labeled DNA and low frequency electric fields for enhancing the fluorescence intensity

The interaction of gold nanoparticles with external electric fields is dependent on the applied frequency, and the dielectric properties of the buffer. The charging frequency $(f_{\rm CH})$ for the gold-electrolyte is calculated using, $f_{\rm CH} = \frac{2\Pi}{\frac{gl}{M\tau}}$, where Iis the diameter of the nanosphere, λ is the Debye length, ε and σ is the electrical permittivity and the conductivity of the buffer, respectively [37]. fch for 20 nm diameter spherical and 30 nm long with 10 nm diameter rod shape commercially available gold nanoparticles suspended in the $0.01 \times TE$ was 20 MHz and 14 MHz, respectively. When the applied frequency is below f_{CH} , the double layer of the metal electrolyte is fully charged, and electric field lines surround the metal nanoparticle. In this case, the electric field distribution around the nanoparticle is identical to the electric field around a dielectric particle [37]. The electric field distribution around the gold nanoparticle produces ∇E^2 and subsequently produces DEP force on surrounding molecules. We have developed a COMSOL calculation and calculated the electric fields and ∇E^2 around the spherical and nanorod particles used in experiments (figure 3(a)). Larger electric fields and their gradients were produced in the areas that had smaller background electric field. For example, a maximum of about 5fold increase in the electric field gradient is possible in the region shown in the rectangle in figure 3(a). In comparison, we have found that no ∇E^2 enhancement (or enhancement is ~ 1) due to the nanoparticles in the straight arm of the T-electrode where local electric is very high (>8 \times 10⁵ V m⁻¹). This calculation demonstrates that gold nanoparticles can effectively be used to produce local high electric fields and their gradients, especially in the regions that have smaller background electric fields. This result highlights the feasibility of

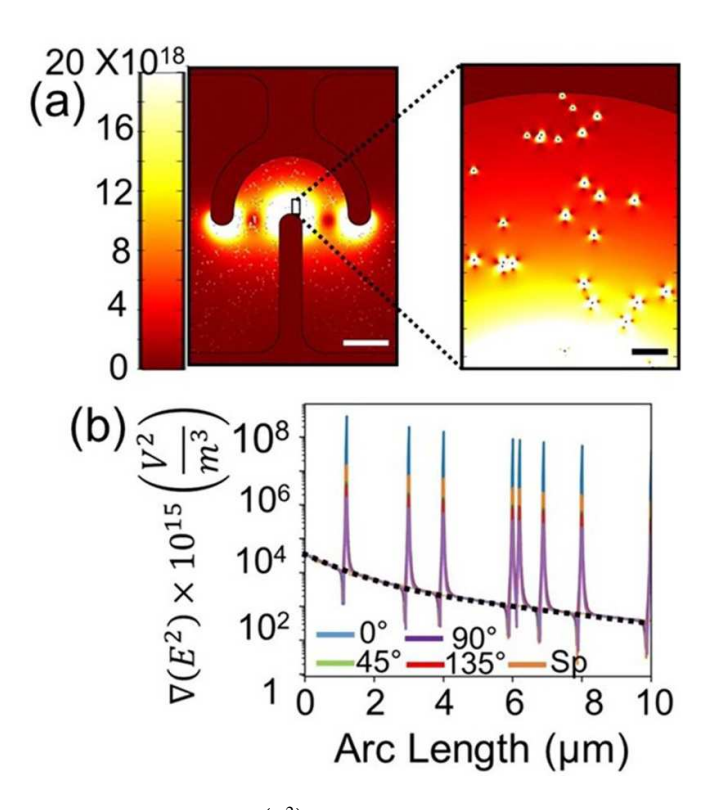


Figure 3. Calculated $\nabla\left(E^2\right)$ in the device when nanoparticles are present. (a) Calculation discussed in figure 1(b) was extended to calculate $\nabla\left(E^2\right)$ for 87×10^9 particles ml^{-1} pipetted on the electrode. Inset illustrates the zoomed view of the calculated local $\nabla\left(E^2\right)$ distribution around the nanospheres. Scale bars represent $10~\mu\mathrm{m}$. (b) Calculated $\nabla\left(E^2\right)$ along randomly selected contour line demonstrates the effects of nanorod orientation (major axis) with the applied electric field. Broken line shows the variation of $\nabla\left(E^2\right)$ without nanoparticles.

locally concentrating fluorophore labeled DNA molecules on the nanoparticles particularly in the regions far away from the electrodes where local ∇E^2 produced by the electrodes are small

To successfully concentrate fluorophore labelled DNA molecules on the nanoparticles, the DEP force produced on molecules must be able to overcome the electrostatic repulsion by the double layer. In general, for spherical nanoparticles, a threshold electric field $(E_{\rm TH}) \approx 1.7 \frac{1}{(K(\omega))} \sqrt{\frac{k_{\rm B}T}{\varepsilon_{\rm p}a^3}}$ where $K(\omega)$ Clausius–Mosotti factor, a is the particle radius, T is the temperature, and $\varepsilon_{\rm p}$ is the permittivity of the particle, is needed [38]. Roughly $E_{\rm TH} \approx 5 \times 10^6 \ {\rm V \ m^{-1}}$ is required for the fluorophore labeled DNA molecules to be trapped on the nanoparticles. We then calculated the minimum background electric field, which is the electric field produced by the electrodes, needed on the surface of the nanoparticle. The electric field around the nanospheres (E_{nano}) for the frequencies $< f_{\text{CH}}$, is given by $-E_0 \cos \theta \left(1 - \frac{a^3}{r^3}\right) \hat{a}_r +$ $E_0 \sin \theta \left(1 + \frac{a^3}{2r^3}\right) \hat{a}_{\theta}$ where E_0 is the applied electric field by the electrodes [39]. By assuming that $r \approx a$, to trap the DNA molecules on the nanospheres, $E_{\text{nano}} > E_{\text{TH}}$ or $\frac{1}{2} \left(\frac{a}{r}\right)^3 >$

 $\left(\frac{E_{\mathrm{TH}}}{E_{\mathrm{o}}}-1\right)$. Based on the dimensions of the nanospheres, $E_0 > 3 \times 10^6 \ \mathrm{V m^{-1}}$ to concentrate fluorophore labeled DNA molecules on the nanospheres. Similarly, E_{TH} and E_0 values for nanorod samples are $7 \times 10^5 \ \mathrm{V m^{-1}}$ and $5 \times 10^5 \ \mathrm{V m^{-1}}$, respectively [40]. By comparing with the calculated electric field values from figure 1(b), nanorods can effectively capture DNA molecules in the area within the circle with white broken lines (see figure 1(d)). In comparison, nanospheres are not very effective in concentrating the DNA molecules as minimum background field of $3 \times 10^6 \ \mathrm{V m^{-1}}$ is needed.

As the DEP force on the DNA molecule is highly dependent on ∇E^2 produced by nanoparticles, we extended our electric field calculation and calculated ∇E^2 variation around nanoparticles (figure 3(b)). Since the nanorod particles may have randomly oriented with the electric fields and distributed throughout the electrode array, we have calculated the variation of ∇E^2 with the angle between the electric field and the major axis of the nanorod and compared the results with nanospheres (see figure 3(b)). We have found that the magnitude of ∇E^2 produced by nanorod particles is dependent on the angle between the electric field and the major axis of the nanorod particles (see figure 3(b)). The maximum and minimum values of ∇E^2 were calculated when the major axis of the nanorod aligns with the electric field (angle is zero) and major axis is perpendicular to the electric field (angle is 90°), respectively. Furthermore, we have found that the greater ∇E^2 values for the nanorods over nanospheres is possible when the angle is less than 45°. Ideally, perfect aligning the nanorods with electric field, which produce the zero angle between the electric field and the major axis, is needed to maximize ∇E^2 produced by nanorod particles. A Torque is needed to align the nanorod oriented with θ degrees with the field. Moreover, the torque is proportional to E^2 and $\sin(2\theta)$. Therefore, we expect that nanorods located in the high electric field regions, e.g. within 'T' section of the electrodes, have a high probability to align with the applied electric field [40].

Once the fluorophore labeled DNA molecules are concentrated on the nanoparticles, DEP force of the nanoparticles was used to concentrate nanoparticles closer to the electrodes. Interactions of low frequency electric fields with metal nanoparticles have been extensively studied and have shown that attractive DEP force is produced by the electric fields <100 MHz. The attractive DEP force concentrates the particles in the highest ∇E^2 or closer to the electrodes. The DEP force to effectively manipulate the nanoparticles, dipole energy exerted by the electric field must be able to overcome thermal energy. The minimum electric field (Es) needed for spherical nanoparticles can be calculated using $\sqrt{\frac{\frac{3}{2}kT}{2\pi\,\varepsilon_m d^3\,\mathrm{Re}(K(\omega))}}$ and found to be at least $10^6~\mathrm{V}~\mathrm{m}^{-1}$ [41]. By comparing the calculated electric field values from figure 1(b), since the electric field values around the nanospheres < 10⁶ V m⁻¹, concentrating nanospheres near the electrodes using DEP force is less likely. In contrast, we have calculated the minimum electric field needed for nanorod particles to be around 10⁵ V m⁻¹. Again, by comparison with calculated electric field values, we have found that nanorod

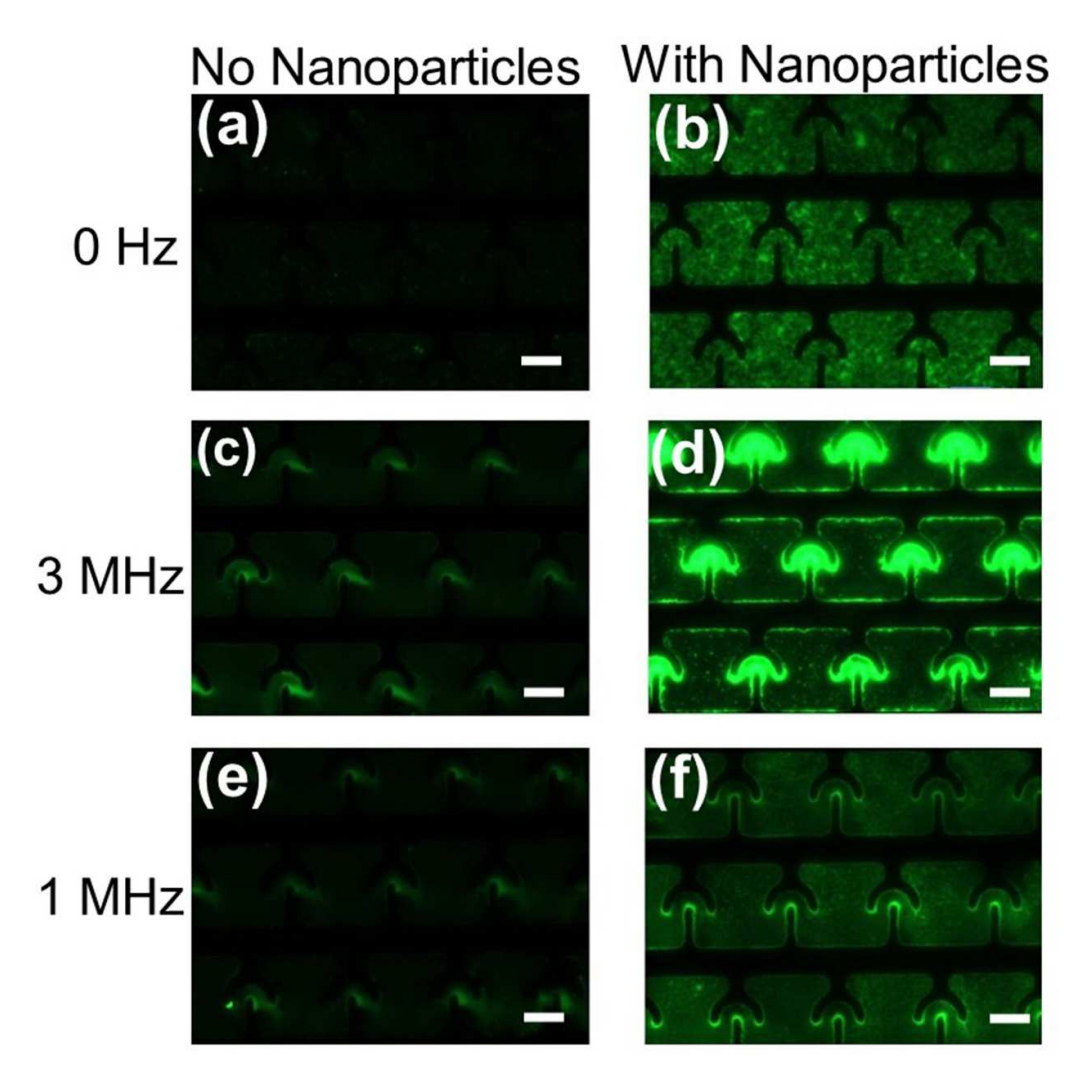


Figure 4. Representative fluorescence images of the AF488 labeled DNA molecules with nanorods and electric fields. (a) Image of the DNA sample on the electrodes with no nanoparticles and/or electric field. (b) Image produced by DNA molecules when nanorods present but, but no electric field was applied. (c) Fluorescence image of the DNA molecules when 10 Vpp (3 MHz) electric field was applied and no nanorod particles were present. (d) Typical image of DNA molecules when 10 Vpp (3 MHz) electric field applied and nanorod particles were also present. (e) Fluorescence image of the DNA molecules when 10 Vpp (1 MHz) electric field was applied. (f) Fluorescence image of the DNA molecules and nanorods when 10 Vpp (1 MHz) electric field was applied.

particles can effectively be concentrated using the DEP force. Therefore, the experiments conducted with nanorod particles can expect a greater impact on the fluorescence enhancement.

In figure 4, we presented additional evidence to support the claims discussed above. Figure 4(a) illustrates the image of the sample when the fluorophore (AF488) labeled DNA molecules were directly pipetted on to the electrodes. There was no significant concentration of fluorophore labeled DNA molecules on the electrodes. We expect that there can be few molecules that can benefit from the interaction of plasmons and enhance the fluorescence intensity. Figure 4(b) illustrates the image when nanorods were introduced with fluorophore labeled DNA molecules, but no electric field (3 MHz) was applied. The fluorescence intensity of DNA molecules located near the nanorods can be enhanced by the interaction of fluorophores molecules and localized surface plasmons. The bright fluorescence spots in the image could be due to the local

fluorescence enhancement by surface plasmons. Fluorophore quenching can also take place in these experiments, especially, when the fluorophore molecules are located <5 nm from the nanorods. Figure 4(c) was recorded when an electric potential of 10 Vpp (3 MHz) was applied to the electrodes but there were no nanorods presented in the sample. Fluorophore labeled DNA molecules could still utilize the electric field (e.g. DEP force and EOF) and concentrate on the T-electrodes. We expect a minimum fluorophore quenching due to the application of the electric field. Figure 4(d) illustrates the image of the sample recorded when both nanorods and electric field were presented (10 Vpp at 3 MHz), which produced the highest fluorescence intensity. This could be due to concentration of fluorophore labeled DNA on the nanorods, concentration of nanorods in T electrodes, fluorescence enhancement and reduction of fluorophore quenching by the electric fields. We performed additional experiments using the

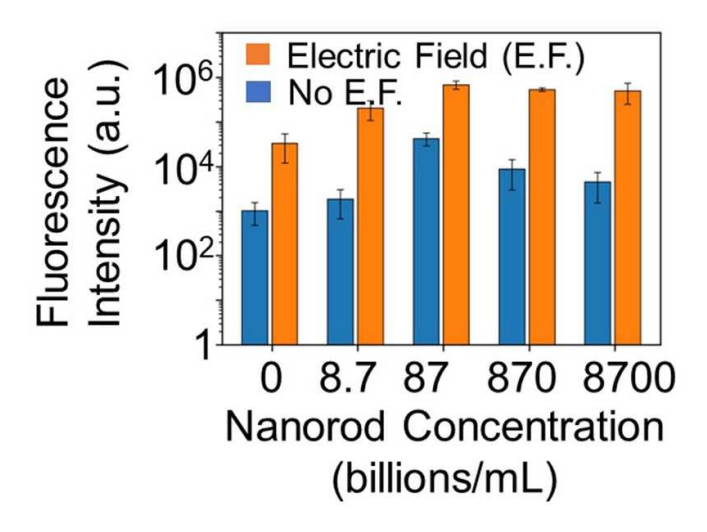


Figure 5. Experimentally measured variation of fluorescence intensity of fluorophore labeled DNA molecules (AF488) with nanorod concentration and the DEP force on fluorophore labeled DNA molecules and nanorods.

electric field produced using 10 Vpp and 1 MHz. Figure 4(e) illustrates fluorophore labeled DNA concentrated at 1 MHz with no nanorods presented. As discussed earlier, in comparison to 3 MHz, the DEP force on the DNA molecules is weaker at 1 MHz. Therefore, less concentration of DNA molecules can be expected. Figure 4(f) shows the image recorded for the fluorophore DNA with nanorods with 1 MHz electric field. In this frequency, concentration of fluorophore labeled DNA on the nanorods and the concentration nanorods in the T-electrodes were not effective. Slight increase in fluorescence in the 'T' electrode are compared to the outside of the 'T' regions could be due to concentrated nanorods enhancing fluorescence intensity local DNA molecules.

Next, we studied fluorescence intensity of DNA molecules when gold nanorod particles and electric fields (3 MHz) are present. Moreover, we carried out additional experiments using various concentrations of nanorods to study the interaction of localized surface plasmons, fluorophore dipoles and electric fields (figure 5). The fluorescence enhancement values we calculated using the experimentally measured intensity values. In the first experiment, we measured the fluorescence intensity of fluorophore labeled (AF488) DNA molecules with and without applying an electric field (10 Vpp at 3 MHz). In average, we have found that about 30-fold increase of fluorescence intensity with the introduction of electric field (3 MHz). This increase could be due to the concentration of fluorophore labeled DNA molecules in the electrodes and the reduction of fluorophore quenching by the electric field. In the next experiments, we varied the concentration of nanorod particles and measured the fluorescence intensity with and without the electric field (figure 5). We have found that when electric field was absent, fluorescence intensity increases with the nanorod concentration from $0-87 \times 10^9$ particles ml⁻¹ and gradually decreased for the concentrations higher than 87×10^9 particles ml⁻¹ (see figure 5). The fluorescence intensity can be treated as a function of internanorod distance and the distance between nanorod and DNA molecules. The former enhances the fluorescence intensity by increasing the local excitation rate, and the latter will decrease the fluorescence intensity by quenching. The increase in the fluorescence intensity from 0 to 87×10^9 particles ml⁻¹ could be due to decreasing the interparticle distance and subsequently increasing the number of plasmonic hotspots. This nanorod concentration range (from $0-87 \times 10^9$ particles ml⁻¹) can be called fluorescence enhancing concentrations as in this region, we expect fluorophore quenching at a lesser degree. In these concentrations, the most of fluorophore labeled DNA molecules are still far from the quenching region of nanoparticles (>5 nm). As the concentration of nanorod increases, interparticle distance decreases and subsequently fluorophore-nanorod distance decreases. When nanorod concentration $>87 \times 10^9$ particles ml⁻¹, fluorophore quenching become more dominant mechanism, and as a result, a decrease of fluorescence with increasing the nanorod concentration was observed. Another important consideration is the number of fluorophore-labeled DNA molecules per nanorod. For example, if there is excessive number of DNA molecules associated with nanorod, inter molecular electrostatic repulsions will keep some DNA molecules outside of the fluorophore quenching or enhancement regions. These molecules will not have any impact due to the nano-rods.

In comparison, when electric field is applied (10 Vpp, 3 MHz), in comparison with no electric field case, higher fluorescence values were recorded. Higher fluorescence intensity with the introduction of electric field could be due to the reduction of the interparticle distance, concentration of fluorophore DNA in nanorod particles and the reduction of fluorophore quenching by 3 MHz electric fields. Additionally, there is a gradual increase in the fluorescence intensity with nanorod concentration from $0-87 \times 10^9$ particles ml⁻¹. Surprisingly, when the nanorod concentration $> 87 \times 10^9$ particles ml⁻¹, the fluorescence intensity did not significantly vary with the nanorod concentration. This could be due to the reduction of the quenching by the electric field by placing the fluorophore molecules outside the quenching region. When fluorophore quenching is minimized, one would expect an increase in fluorescence with an increase in concentration. In this nanorod concentration range, there could be no significant variation of fluorophore molecules per nanorod. Therefore, increasing the nanorod concentration beyond 87×10^9 particles ml⁻¹ will have a little impact on increasing the fluorescence intensity. Overall, maximum of 125-fold (for 87×10^9 particles ml⁻¹) fluorescence enhancement was recorded when the electric field was applied.

To further study the effects of low frequency electric fields on the enhancement of fluorescence intensity, we performed additional calculations and experiments. Broadly, fluorescence enhancement (G) at a point in the device that is located outside of the quenching region (>5 nm) can be expressed as,

 $G \sim G_{\rm EX}G_{\rm QY}$, where $G_{\rm EX}$ is the enhancement due to the increase in the excitation rate by the local electric fields produced by the plasmons of gold electrodes and nanoparticles,

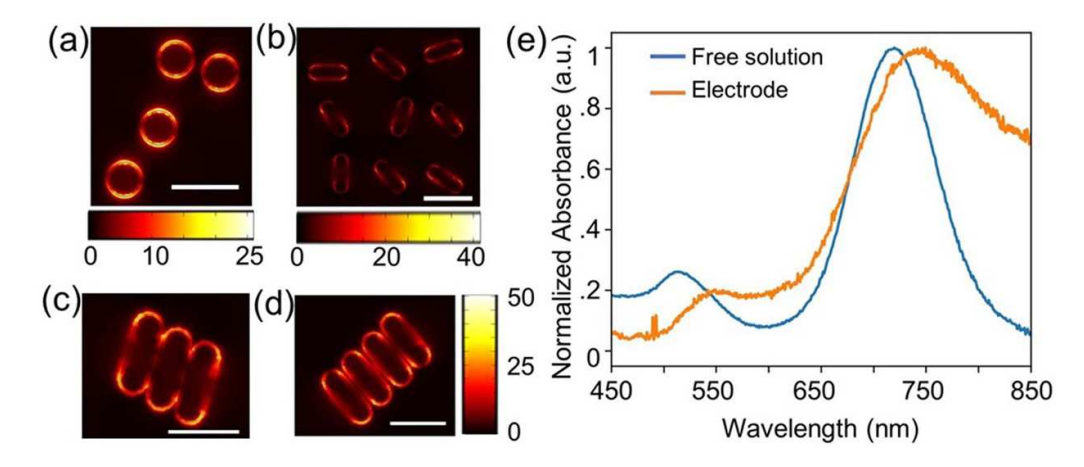


Figure 6. Characterization of nanospheres, and nanorod-electrode combination. (a) Top view (x-y) plan illustrates the calculated electric field around single nanospheres due to excitation of localized surface plasmons by the incident light (z-direction). The scale bar shows 20 nm. (b)–(d) Calculated electric field distribution in the x-y plan of single and clustered nanorods due to the excitation of localized surface plasmons by the excitation light (z-direction). Scale bars show 20 nm. (e) Variation of absorbance values with wavelength (450–850 nm) for single nanorods, and nanorods and T-electrodes.

fluorophore molecules [42]. The excitation light excites the surface plasmons of spherical and rod-shaped nanoparticles and produce local high electric field regions, which is dependent on the size and shape of the nanoparticles with respect to the wavelength of the excitation light. In addition, the excitation light excites the surface plasmon modes of gold electrodes and produces SPPs. The strength of the electric fields produced by the surface plasmons of the nanoparticles are highly localized and approximately dependent on R^{-3} , where R is the distance between the center of the nanoparticle and the point of interest [43]. To study the expected local electric fields produced by the surfaced plasmons of spherical and rod shape nanoparticles, we have developed a COMSOL calculation and solved the wave equation. We have then extended the calculation and calculated the enhanced electric field near the nanoparticles by dividing the calculated electric field (E) near the gold nanoparticles by the background electric field (E_0) . Finally, the magnitude of $G_{\rm EX}$ was calculated using $\left(\frac{E}{E_0}\right)$ [9]. Figures 6(a)–(d) illustrates the calculated G_{EX} for nanospheres and nanorods. This calculation demonstrates that the nanorods produce higher $G_{\rm EX}$ than that of nanospheres (25 vs. 50). Furthermore, in addition to single particles, nanorod and nanosphere samples formed clusters when placed them on the electrodes (figure S2). To study the electric fields produced by particle clusters, we have extended our calculation to a few nanorod clusters. We have found that in comparison with single nanorod particles, clustering produces larger electric fields and increases $G_{\rm EX}$ (e.g. 40 vs. 50).

and G_{OY} is the enhancement due to the increasing QY of the

The nanorods were placed throughout the electrodes, and to characterize plasmonic interactions between nanorods and, nanorod and electrodes, we have performed additional experiments using absorbance spectroscopy. We measured the absorbance spectra of nanorod samples with and without electrodes (figure 6(e)). When there was no electrode, single nanorods show two distinct peaks at 525 nm and 725 nm.

These absorbance peaks correspond to longitudinal (725 nm) and transverse (525 nm) plasmon resonance values. The maximum expected absorbance peak (λ_m) can be calculated using $\lambda_{\rm m} = 95R + 420$, where R is the aspect ratio of the nanorods and found that $\lambda_{\rm m} \approx 705$ nm, which is approximately equal to what we have experimentally observed [44]. As discussed earlier, when we placed the nanorods in the electrodes, a majority of nanorods can form complex structures eighter connecting nanorods side-by-side (along the minor axis) or end-to-end (along the major axis). However, the scanning electron image (see figure S2) shows that a significant portion of the nanorods deposited on the electrodes form complex structures by connecting single nanorods side-by-side. These complex structures make plasmonic coupling between adjacent nanorods and with T-electrodes and produce blue- or redshifts to the absorption peaks produced by single nanorods. Previous studies have reported that just side-by-side formation of nanorods (with no electrode) produce blue-shift on the longitudinal band (725 nm) and red shift in the transverse band (525 nm) [45]. Surprisingly, when we measured the absorbance of the nanorods with T-electrodes, we measured red shifts in both longitudinal (\sim 50 nm) and transverse bands (\sim 25 nm). In comparison with findings reported in [35], we have found that presence of electrodes has no impact on the transverse band, but longitudinal band produced a opposite result (blueshift vs. red-shift). This anomalous result, especially in the longitudinal band, could be attributed to the plasmon coupling formed between complex nano-rod-electrode structures. This data suggests that plasmon coupling between the nanorods and electrodes could have an impact on $G_{\rm EX}$ values, especially near the electrodes. When low frequency electric field (3 MHz) is used, as discussed earlier, nanorods are brought closer to the electrodes and therefore fluorophore molecules could use the higher $G_{\rm EX}$ values to enhance the fluorescence intensity. Later in the study, we will discuss the fluorescence enhancement of fluorophores excited by these structures.

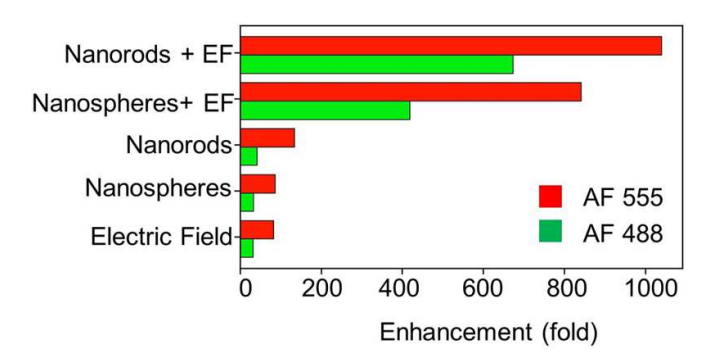


Figure 7. Experimentally measured fluorescence enhancement variation of DNA labeled with low (AF 555) and high (AF 488) quantum yield fluorophore molecules with electric fields, DEP forces on DNA molecules and nanoparticles.

The momentum of the SPP mode is aways in the interface of the gold and dielectric, which is greater than the momentum of the photon in the dielectric medium. Therefore, SPP mode is non-radiative [43]. The non-radiative decay process flows energy from the excited fluorophore molecule into its surroundings, including to gold T-electrodes [43]. Weber and Eagen have demonstrated that a significant amount of energy of the excited molecules is lost to SPPs as non-radiative decay which contributes to the fluorophore quenching [46]. For example, the energy flow from a fluorophore molecule to a dipole (e.g. gold electrode) is dependent on the distance between the fluorophore and the dipole (d). Moreover, the nonradiative decay falls as d^{-3} [43, 47]. As energy flows out of the fluorophore molecules, QY of the fluorophore molecules decreases. As discussed in the previous section, the utility of electric fields keeps the fluorophore labeled molecules out of the fluorophore quenching region. Therefore, the expected contribution from SPP is not very significant [46, 47].

Next, we studied the effects of low frequency electric fields on G_{OY} . The experiments were carried out using DNA molecules labeled with low QY (AF555, QY = 0.1) and high QY (AF488, QY = 0.9) fluorophore molecules and calculated the fold increase of the fluorescence intensity with various experimental conditions (figure 7). Theoretically, based on the intrinsic values of QY, we expect a significant improvement to the low QY fluorophore labeled DNA molecules. For example, an increase in QY from .1 to 1 will result in 10fold fluorescence intensity increase. At the same time, only \sim 1.1-fold increase of fluorescence intensity is possible for the DNA molecules label with AF488. First, we performed experiments by pipetting fluorophore (AF488 and AF555) labeled DNA molecules (no nanorod particles) directly on the electrodes, applying electric field and calculating the fluorescence enhancement folds for each fluorophore (see 'Electric Field' bar charts). Since the QY of AF488 is close to 1, the fluorescence enhancement associated with AF488 labeled DNA could entirely be due to the concentration effect and minimizing the fluorophore quenching. In comparison, fluorescence enhancement of AF555 labeled DNA molecules could be due to concentration effect, minimizing the quenching and the improvement of QY. If we assumed an increase of QY of AF555 from .1 to 1, we could expect about (~1/.1) 10-fold increase in fluorescence intensity. This would result at least in about a 10-fold improvement of signal-to-noise ratio. Experimentally recorded total enhancement for AF555 was about 100-fold (see 'Electric field' bars in figure 7). Since AF488 molecules have very high QY and have a minimum room (increasing from .9 to 1) for improvement of the QY, the recorded 50-fold enhancement may primarily be due to the concentration effects by the field. When we take ratio between the fluorescence enhancements of AF555 and AF488, we have found that about 2-fold enhancement of AF555 over AF488. The 2-fold enhancement could be due to the improvement signal to noise ratio.

Next, we studied the enhancement of fluorescence due to the presence of nanoparticles. We performed experiments using nanorods and nanospheres labeled with AF555 and AF488 molecules (see bars labeled as 'nanospheres' and 'nanorods') but no electric fields were applied. Therefore, electric field mediated fluorescence enhancement, including the reduction of fluorophore quenching and increase of Q_{YE} are not expected to occur. However, the fluorophore labeled DNA molecules located closer to the electrodes and nanoparticles are expected to interact with plasmons and increase $Q_{\rm YE}$. In comparison, regardless of the nanoparticle shape, larger enhancement values were recorded for AF555 labeled DNA molecules. The largest enhancement was recorded for AF555 labeled DNA molecules with nanorods. To understand the fluorescence enhancements produced by low and high QY fluorophore labeled DNA molecules, we calculated fold enhancements (using $\left(\frac{AF555}{AF488}\right)$) of 2.25- and 3-folds for nanospheres and nanorods, respectively. From this result, it can be concluded that nanorods are marginally better than nanospheres in improving fluorescence intensity without 3 MHz electric field. In addition, the fluorescence enhancement of AF488 suspended in nanospheres and nanorod samples were roughly 60- and 50-folds, respectively. As noted above, the fluorescence enhancement of high QY molecules is primarily by $G_{\rm EX}$. This result shows that nanospheres are slightly better than nanorods in increasing the fluorescence intensity by $Q_{\rm EX}$.

In the next experiment, we studied the fluorescence enhancement due to the presence of nanoparticles and electric field (3 MHz). As discussed previously, when the electric field at 3 MHz is applied, no DEP force is expected to be produced on nanospheres (see bar labeled as 'nanospheres + EF' in figure 7) but fluorophore labeled DNA molecules experience a strong DEP force. Using the fluorescence enhancement of the 'nanospheres' and 'nanospheres + EF' bars, calculated enhancements (using $\left(\frac{\text{nanospheres} + \text{EF}}{\text{nanospheres}}\right)$) were 14 and 7-folds for nanospheres AF488 and AF555, respectively. Note that higher enhancement fold was reported for high QY fluorophores or AF488. This data shows that the electric fields and the DEP force of the DNA molecules contributed to the fluorescence enhancement of AF488 labeled DNA molecules. This enhancement could be attributed to the increasing G_{EX} and minimize the quenching.

Finally, we studied the fluorescence enhancement due to the presence of electric field and DEP forces of DNA molecules and nanoparticles (see bars labeled as 'nanorods' and 'nanorods + EF' in figure 7). We calculated the enhancement in folds using $\left(\frac{\text{nanorods} + \text{EF}}{\text{nanorods}}\right)$ and obtained 9 (fold enhancement) for AF488 and AF555 labeled DNA molecules. In comparison with previous experiments, combination of electric fields and DEP forces of nanoparticles and DNA molecules enhance the fluorescence intensity of AF555. through G_{OY} and make it equal to the enhancement from $G_{\rm EX}$. This result shows that the need of electric field and the DEP force of both DNA molecules and nanoparticles for enhance the fluorescence intensity of AF555. Overall, the largest enhancement (over 1000-fold) was reported for the AF555 labeled DNA molecules suspended with nanorods and 3 MHz electric fields. In comparison, about 700-fold enhancement was reported for the AF488 labeled DNA molecules with nanorods and DEP force on nanorods and DNA molecules.

To understand and provide a plausible explanation on how low frequency electric field at 3 MHz enhances the QY of the fluorophore molecules, we have utilized the work developed by Chance et al, where a classical approach was developed to calculate the effects of radiation fields from a reflecting metal surface and subsequently calculated the lifetime of a nearby emitter molecule (e.g. fluorophore molecule) [48]. Moreover, classical equations of motion were developed for oscillating dipole in the presence of the reflected electric field (E_R) by the metal surface, where $E_{\rm R}=E^0{\rm e}^{-i\Omega t}$, E^0 and Ω are the complex electric field magnitude and frequency, respectively. Using the work developed by Chance et al, we calculated the lifetime of the fluorophore molecules when its dipole axis aligned perpendicularly and parallel with E_R . We have assumed that metal have perfect reflection of incident light and used $E_{\perp}^o = \frac{\mu_0}{n_1^2} \left[\left(\frac{2}{\sigma^3} - \frac{2ik_1}{\sigma^2} \right) e^{ik_1\sigma} \right]$ and $E_{=}^o = \frac{\mu_0}{n_1^2} \left[\left(\frac{1}{\sigma^3} - \frac{k_1^2}{\sigma} - \frac{ik_1}{\sigma^2} \right) e^{ik_1\sigma} \right]$ for perpendicular and parallel components of the reflected electric field, respectively, where σ and n_1 are the distance between the dipole and its image and n_1 is the index of refraction of the medium containing the dipole, respectively. Additionally, $k_1 = \Omega n_1/c$ and μ_0 is the maximum dipole moment of the dipole or fluorophore molecule. We used the expression derived by Chance *et al*, to calculate the lifetime (τ_D) when

metal is present, which is
$$\tau_D = \left[\frac{1}{1 + \frac{3Y_0c^3}{2\mu_0\eta_1\omega^3} \text{Im}E^0}\right] \tau_0$$
 where τ_0 is the lifetime when metal is absent. Y_0 is the OV of the fluore.

the lifetime when metal is absent, Y_0 is the QY of the fluorophore when metal is absent, and c is the speed of light and ω is the frequency of oscillation of the fluorophore dipole [48]. We calculated the expected improvement (increase or decrease) to QY, $Y = \frac{1}{\tau_D}$, of the fluorophore molecule when the fluorophore dipole axis is perpendicular and parallel to the reflected electric field (table 1). Moreover, we assumed that $\sin{(k_1\sigma)} \approx 0$ and $\cos{(k_1\sigma)} \approx 1$ when σ is small, and $\sin{(k_1\sigma)} \approx 1$ and $\cos{(k_1\sigma)} \approx 0$ when σ is bigger.

As the calculation shows, the alignment of fluorophore dipole axis, ideally in the direction of the perpendicular electric field, can have dramatic improvement to the QY. In addition, these fluorophore molecules need to be outside the

Table 1. Expected effects to the quantum yield of fluorophore molecule when gold is presented.

Condition	Smaller σ	Bigger σ
E0= E0⊥	· •	$Y_0 < Y_{D1}$ (enhancement) $Y_0 \ll Y_{D2}$ (significant enhancement)

'smaller σ ' region. Classically, when the distance between the fluorophore dipole and metal <5 nm, an image dipole on the metal is produced in the opposite direction and the net dipole strength of the fluorophore and its image could be less than the intrinsic dipole strength of the fluorophore and reduce the QY. As we discussed earlier, when 3 MHz electric fields are used, the combination of DEP force and the EOF increases the separation between the metal and the fluorophore and minimizes the fluorophore quenching. When d > 5 nm, theoretically, if the dipole is aligned eighter with perpendicular or parallel components of the reflected electric field, the result is the addition of the image dipole and fluorophore dipole and increase the net dipole strength and subsequently improve the QY. When the low frequency electric fields are used, especially at 3 MHz, DNA molecules are polarized, and the induced dipole moment of the DNA molecules (P) is given by $\vec{P} = \alpha \vec{E}$ where α is the total polarizability of the DNA molecule, and the E is the applied electric field. The electric field produces a torque (T), $\vec{T} = \vec{p} \times \vec{E}$ on DNA molecules [49]. This torque causes the DNA molecule to stretch and align its long axis with the low frequency electric field. The induced dipole on the DNA molecule produces a local electric field (E_d) , $E_d \approx -\frac{\vec{p}}{4\pi \, \varepsilon r^3}$, where r is the distance between the dipole and the observation point [39]. We have roughly calculated the $E_{\rm d}$ to be around $1 \times 10^9 \text{ V m}^{-1}$ within 10 nm radius from the dipole. Since $E_{\rm d}\gg E$, regardless of the fluorophore polarizability with the low frequency electric field, due to the presence of very large $E_{\rm d}$, a torque can be produced on the fluorophore molecules that are conjugated to the DNA molecules and aligns with the direction of E_d . Since the E_d and external electric field (E) is aligned with each other, fluorophore dipole could also be aligned with the externally applied low frequency electric field or *E*.

When nanoparticles are present, to achieve the maximum possible fluorescence intensity, the alignment of fluorophore dipole axis with reflected electric fields (or $E_{\rm R}$) produced by nanoparticles is needed. Moreover, the extent of the alignment can be described using the alignment angle (θ) that is dependent on the value of $\cos^{-1}\frac{E_{\rm R}.E}{|E_{\rm R}||E|}$ and α is dependent on the particle shape and equal to $\tan^{-1}\frac{E_{\rm u}^0}{E^0}$. Ideally, when $\alpha\approx90^\circ$, $\theta\approx0^\circ$ is needed to significantly enhance the QY. Similarly, for smaller values of α , $\theta\approx90^\circ$ is needed. The value of α is dependent on the nanoparticle shape and the lower and upper limits of the QY will be Y_{D1} and Y_{D2} , respectively. For example, if a particle produces $E_{\perp}^0\gg E_{-}^0$ and $\theta\approx90^\circ$, QY will be equal to Y_{D2} . Similarly, Y_{DI} is reached when $E_{-}^0\gg E_{-}^0$ and $\theta\approx0^\circ$. When compare the enhancement values calculated from the experiments reported in figure 7, we found that

the fluorophore molecules suspended in nanosphere molecules may not be effectively aligned with the externally applied low frequency electric fields (3 MHz) or E. In comparison, fluorophore molecules suspended with nanorod samples better aligned with the plasmon electric field produced by the nanorods. Additionally, DEP force is produced on nanorod particles and moves nanorods toward electrodes. As we discussed previously in figure 6(e), complex structures of electrodes-nanorods are produced. These complex structures could produce larger $G_{\rm EX}$ values than those with no DEP force. For example, as shown in figure 7: 'nanospheres + EF' vs. 'nanorods + EF', we have found that enhancement of AF555 labeled DNA molecules with nanorods, and DEP force produced larger enhancement than the nanospheres with no DEP force (1050 vs. 850).

3. Conclusions

Our experimental results and calculations demonstrate the utility of low frequency electric fields to enhance the fluorescence intensity of fluorophore molecules. In addition, we also studied the effects of low frequency electric fields to minimize fluorophore quenching. The selection of the frequency of the low frequency electric field should be based on the charging frequency of the biomolecules and the nanoparticles. One can determine the size of the nanoparticle based on the charging frequency of the nanoparticle and biomolecule. The utility of commercially available gold nanoparticles eliminates the need for expensive e-beam lithography-based nanostructure manufacturing. Additionally, to achieve the maximum possible fluorescence enhancement, in addition to the selection of the frequency, a careful selection of buffer conductivity, nanoparticle concentration and QY of the fluorophore molecules needed to be done. Although this study was focused on fluorophore labeled short DNA molecules, the results can be extended to other molecules (e.g. antigen) and beyond. For example, to detect antigen molecules suspended in 0.01x TE buffer, the frequency of external electric field needs to be about 600 KHz [50]. Finally, the new knowledge on particle and molecular manipulation and fluorescence enhancement can be utilized in a wide range of applications, including biosensor development.

4. Materials and methods

4.1. Procurement of fluorophore labeled DNA molecules, nanoparticles, and chemicals

Alexa Fluor 488 (AF488; QY: 0.92, excitation max: 490 nm, emission max: 525 nm) conjugated single-stranded DNA molecules (5'-(AF488 NHS)(5'-amino c6)AACTATACAACCTACTACCTCA-3) was purchased from Midland Certified Reagent Company Inc. (Midland, Texas, USA) and Alexa Fluor 555 (QY: 0.10, excitation max: 555 nm, emission max: 580 nm) conjugated single stranded

DNA (5'-/5Alex555N/AACTATACAACCTACTACCTCA-3') was purchased from Integrated DNA Technologies, Inc. (Coralville, Iowa, USA). Au nanorods (A12-10-700-CTAB-DIH-1-25) and Au nanospheres (A11-20-CIT-DIH-1-10) suspended in 18 M Ω DI water was purchased from Nanopartz Inc. (Loveland, CO, USA). The average diameter and length of the Au nanorods are 10 and 30 nm, respectively and the average diameter of the nanospheres is 20 nm. Tris-EDTA (TE) buffer (pH 8.0) was purchased from Integrated DNA Technologies, Inc. (Coralville, Iowa, USA).

4.2. Nanoparticle assembling

Au nanoparticles were assembled on the TIE using the solvent evaporation-induced assembly method. 10 μ l of Au nanoparticles suspended in DI water was pipetted on the TIE and let the DI water dry in ambient conditions. After around 40 mins, the DI water was dried, and Nano-particle assemblies were obtained. To dilute the nanoparticles or to obtain nanoparticle concentrations lower than the supplier, the nanoparticles were diluted in DI water to achieve the desired concentrations. To enrich the nanoparticles, or to obtain nanorod concentrations higher than the supplier provided, 1 ml of the supplier provided nanoparticles were centrifuged at 10 000 rounds per minute for 2 min and desired solute volume was removed to achieve the required concentration.

4.3. Molecular concertation experiments and fluorescence enhancement calculation

Alexa Fluor conjugated ssDNA samples were suspended in 0.01x TE buffer (15 μ S cm⁻¹) to archive the concentrations from 10 μ M to 1 nM. 10 μ l of DNA sample were pipetted on the TIE or TIE + nanoparticle assemblies or on plain glass slides. As soon as the samples were pipetted, sinusoidal waveforms with 10 Vpp (frequency: 0, 1, 3, or 5 MHz) were applied to the TIE electrodes. Approximately after 15 mins of electric fields, the samples were dried. For the samples without applied electric potential, the drying time was about 40 mins in ambient conditions. Thereafter devices or microscope glass slides were imaged using an inverted fluorescence microscope (XD30A-RFL, Ningbo Sunny Instruments Co., Ltd, Zhejiang, China). Moreover, fluorescent images were recorded using 40× magnification with CCD Fluorescent Microscope Camera (MT5000 (IFR), AmScope, CA, USA). ImageJ (National Institutes of Health, Bethesda, USA) software was used to obtain color intensity values of fluorescence images. Briefly, each image was imported to ImageJ separately and histogram of fluorescence intensity was plotted. Then the total enhanced pixel fluorescence intensity value was calculated by multiplying the color intensity by the corresponding number of pixels and summing the values in the enhanced region. Color intensities below 100 were considered as background and only the values from 101 to 255 were utilized to calculate the total enhanced pixel fluorescence intensity of each image.

4.4. Scanning electron microscopy imaging

Electrodes with nanoparticle assemblies were attached to aluminum mounts with copper adhesive tape (Ted Pella, Inc., CA, USA) and coated with a minimum conductive layer of carbon in a high-vacuum evaporative coater (Cressington 208c, Ted Pella Inc., CA, USA). Images were recorded using scanning electron microscope (JEOL JSM-7600F, JEOL USA Inc., MA, USA).

4.5. Absorbance spectra recording

Absorbance spectra of Au nanorods and Au nanospheres were recorded using spectrophotometer (Cary-60 UV-Vis, Agilent, Santa Clara, CA or DU 530, Beckman Coulter, Indiana, USA). Spectra were also recorded for 200 μ l of the Nanorods and nanospheres in DI water as well as assembled on TIE considering nanoparticles (8.7 × 10¹⁰ nps ml⁻¹).

4.6. Fluorescence enhancement factor calculation

Experiments were carried out using no nanoparticles (nanorods and nanospheres) and no electric fields, electric fields (1 and 3 MHz) but no nanoparticles, nanoparticles (nanospheres and nanorods) and no electric fields, and electric fields (1 and 3 MHz) and nanoparticles (nanospheres and nanorods). All the experiments were performed using 1 μ M ssDNA molecules labeled with AF 488 and AF555 molecules. Total enhanced pixel fluorescence intensity was calculated for each experiment using the method outlined above. Finally, to calculate the enhancement in fold for an experiment, the calculated total enhanced pixel fluorescence intensity value was divided by the calculated total enhanced pixel fluorescence intensity of no nanoparticle and no electric field experiment.

After the average effective fluorescence intensity is calculated for each condition with 1 μ M Alexa fluor ssDNA samples the enhancement factors were calculated by dividing the average effective fluorescence intensity by effective fluorescence intensity corresponding to no nanoparticle no field condition for AF488 and AF555 respectively.

4.7. Electric field and electric field gradient calculation

The electric field, and field gradient $(\nabla |E|^2)$ on the TIEs were calculated using AC/DC module of COMSOL Multiphysics software (COMSOL Inc., MA, USA). First, TIEs were drawn according to the scale (AutoCAD; Autodesk, Inc., CA, USA) and imported to COMSOL. The 2D drawing was extruded by 100 nm and added an outside boundary to the geometry. It was assumed that 0.01x TE (15 μ S cm $^{-1}$) was around the TIEs. The meshing of the 3D geometry was done using physics-controlled meshing and electric potential (ν) across the array of electrodes. The electric field ($E=-\nabla \nu$), and the electric field gradient were calculated considering the TIE in XY plane at 50 nm of the Z plane by applying 10 Vpp voltage to the electrodes.

Above calculations were extended when nanorods and nanospheres were presented. Nanorods and nanospheres were added to the geometry using the geometry options available in COMSOL. The orientations of the nanorods were randomly selected and nanoparticles were drawn according to the scale. The geometry was meshed as extremely fine meshing. The boundaries of the nanoparticles were considered as floating potential groups, such that there is constant voltage V_0 is applied on the boundaries with total normal electric displacement field (D) equals to a specific charge Q_0 ,

$$V = V_c$$

$$\int_{\partial\Omega}^{\Box} (D.n) \, dS = Q_0$$

where Ω and n represent the boundary, and surface normal respectively. Electric field and their gradients were calculated when 10 Vpp potential is applied to the electrodes. This calculation was repeated to calculate the electric field gradient values when the major axis of the nanorods is oriented with 0° , 45° , 90° and 135° with electric fields.

4.8. Electric field enhancement near nanoparticles

The electric fields near the nanoparticles were calculated using the Wave Optics Module, electromagnetic wave in frequency domain studies in COMSOL. Few nanoparticles in random orientations as per SEM observations were drawn to scale using AutoCAD software and imported into the COMSOL Multiphysics. Boundaries were added to the geometry such that, the nanoparticles are placed on quartz substrate and filled with 0.01x TE buffer. The geometry was meshed using the physics controlled meshing technique with extremely fine element size. The excitation light wavelength of 500 nm applied through the substrate and local electric field distribution was calculated. The electric field enhancement was calculated by diving the calculated electric field by the background field (field far away from the nanoparticles).

Data availability statement

No new data were created or analysed in this study.

Acknowledgments

Authors would like to thank Greg Strommen at North Dakota State University for helping in manufacturing T-electrodes used in experiments. DN would like to acknowledge with financial support from Nations Science Foundation (Grant Numbers: 2300064 and 2310106).

Conflict of interest

Authors declare no conflict of interest.

ORCID ID

D Nawarathna https://orcid.org/0009-0008-5463-9172

References

- [1] Strianese M, Staiano M, Ruggiero G, Labella T, Pellecchia C and D'Auria S 2012 Fluorescence-based biosensors Spectroscopic Methods of Analysis: Methods and Protocols (Humana Press) pp 193–216
- [2] Chowdhury A D et al 2020 Controlling distance, size and concentration of nanoconjugates for optimized LSPR based biosensors Biosens. Bioelectron. 170 112657
- [3] Quarin S M, Macke A C, Kissell L N, Kelly M S, Dayananda A, Ungvary J, Stan G, Dima R I and Strobbia P 2023 Design, rationalization, and automation of a catalytic sensing mechanism for homogeneous SERS biosensors ACS Sens. 8 2000–10
- [4] Meeseepong M, Ghosh G, Shrivastava S and Lee N E 2023 Fluorescence-enhanced microfluidic biosensor platform based on magnetic beads with highly stable ZnO nanorods for biomarker detection ACS Appl. Mater. Interfaces 15 21754–65
- [5] Son M H, Park S W, Sagong H Y and Jung Y K 2023 Recent advances in electrochemical and optical biosensors for cancer biomarker detection *Biochip J.* 17 44–67
- [6] Napoletano S, Battista E, Martone N, Netti P A and Causa F 2023 Direct, precise, enzyme-free detection of miR-103–3p in real samples by microgels with highly specific molecular beacons *Talanta* 259 124468
- [7] Nabers A, Hafermann H, Wiltfang J and Gerwert K 2019 Aβ and tau structure-based biomarkers for a blood-and CSF-based two-step recruitment strategy to identify patients with dementia due to Alzheimer's disease Alzheimer's Dementia 11 257–63
- [8] Aslan K, Gryczynski I, Malicka J, Matveeva E, Lakowicz J R and Geddes C D 2005 Metal-enhanced fluorescence: an emerging tool in biotechnology *Curr. Opin. Biotechnol.* 16 55–62
- [9] Velmanickam L, Fondakowski M, Lima I T and Nawarathna D 2017 Integrated dielectrophoretic and surface plasmonic platform for million-fold improvement in the detection of fluorescent events *Biomicrofluidics* 11 044115
- [10] Lakowicz J R 2005 Radiative decay engineering 5: metal-enhanced fluorescence and plasmon emission *Anal. Biochem.* 337 171–94
- [11] Jung Y, Kim J, Kim N H and Kim H G 2023 Ag–ZnO nanocomposites as a 3D metal-enhanced fluorescence substrate for the fluorescence detection of DNA ACS Appl. Nano Mater. 6 976–85
- [12] Zhang J and Lakowicz J R 2007 Metal-enhanced fluorescence of an organic fluorophore using gold particles *Opt. Express* 15 2598–606
- [13] Hong D, Jo E J, Bang D, Jung C, Lee Y E, Noh Y S, Shin M G and Kim M G 2023 Plasmonic approach to fluorescence enhancement of mesoporous silica-coated gold nanorods for highly sensitive influenza A virus detection using lateral flow immunosensor ACS Nano 17 16607–19
- [14] Balevicius Z and Baskys A 2019 Optical dispersions of bloch surface waves and surface plasmon polaritons: towards advanced biosensors *Materials* 12 3147
- [15] Darvill D, Centeno A and Xie F 2013 Plasmonic fluorescence enhancement by metal nanostructures: shaping the future of bionanotechnology *Phys. Chem. Chem. Phys.* 15 15709–26
- [16] Li X and Que L 2014 Fluorescence enhancement enabled by nanomaterials and nanostructured substrates: a brief review *Rev. Nanosci. Nanotechnol.* 3 161–76

- [17] Bek A, Jansen R, Ringler M, Mayilo S, Klar T A and Feldmann J 2008 Fluorescence enhancement in hot spots of AFM-designed gold nanoparticle sandwiches *Nano Lett*. 8 485–90
- [18] Chen G, Wang D, Hong W, Sun L, Zhu Y and Chen X 2017 Fluorescence enhancement on large area selfassembled plasmonic-3D photonic crystals *Small* 13 1602612
- [19] Smolyaninova V N, Smolyaninov I I, Kildishev A V and Shalaev V M 2012 Trapped rainbow techniques for spectroscopy on a chip and fluorescence enhancement *Appl. Phys.* B 106 577–81
- [20] Deng J, Xu J, Ouyang M, Zou Z, Lei Y, Li J, Qing Z and Yang R 2022 Target-triggered hairpin-free chain-branching growth of DNA dendrimers for contrast-enhanced imaging in living cells by avoiding signal dispersion *Chin. Chem.* Lett. 33 773-7
- [21] Song B *et al* 2020 Probing the mechanisms of strong fluorescence enhancement in plasmonic nanogaps with sub-nanometer precision *ACS Nano* **14** 14769–78
- [22] Wang L, Veselinovic M, Yang L, Geiss B J, Dandy D S and Chen T 2017 A sensitive DNA capacitive biosensor using interdigitated electrodes *Biosens. Bioelectron*. 87 646–53
- [23] Velmanickam L, Bains M, Fondakowski M, Dorsam G P and Nawarathna D 2018 iLluminate-miRNA: paradigm for high-throughput, low-cost, and sensitive miRNA detection in serum samples at point-of-care J. Phys. D: Appl. Phys. 52 055401
- [24] Asbury C L and van den Engh G 1998 Trapping of DNA in nonuniform oscillating electric fields *Biophys. J.* 74 1024–30
- [25] Asbury C L, Diercks A H and Van Den Engh G 2002 Trapping of DNA by dielectrophoresis *Electrophoresis* 23 2658–66
- [26] Storey B D, Edwards L R, Kilic M S and Bazant M Z 2008 Steric effects on ac electro-osmosis in dilute electrolytes *Phys. Rev.* E 77 036317
- [27] Nawarathna D, Turan T and Wickramasinghe H K 2009 Selective probing of mRNA expression levels within a living cell Appl. Phys. Lett. 95 083117
- [28] Chou C F, Tegenfeldt J O, Bakajin O, Chan S S, Cox E C, Darnton N, Duke T and Austin R H 2002 Electrodeless dielectrophoresis of single-and double-stranded DNA *Biophys. J.* 83 2170–9
- [29] Talapatra S and Chakraborty S 2008 Double layer overlap in ac electroosmosis *Eur. J. Mech. B, Fluids.* **27** 297–308
- [30] Zhang J, Fu Y, Chowdhury M H and Lakowicz J R 2007 Enhanced Förster resonance energy transfer on single metal particle. 2. Dependence on donor— acceptor separation distance, particle size, and distance from metal surface J. Phys. Chem. C 111 11784–92
- [31] Hariri A A, Newman S S, Tan S, Mamerow D, Adams A M, Maganzini N, Zhong B L, Eisenstein M, Dunn A R and Soh H T 2022 Improved immunoassay sensitivity and specificity using single-molecule colocalization *Nat. Commun.* 13 5359
- [32] Le Ru E C and Etchegoin P G 2009 Phenomenological local field enhancement factor distributions around electromagnetic hot spots J. Chem. Phys. 130 181101
- [33] Carminati R, Greffet J J, Henkel C and Vigoureux J M 2006 Radiative and non-radiative decay of a single molecule close to a metallic nanoparticle *Opt. Commun.* **261** 368–75
- [34] Lin H Y, Tsai L C, Chi P Y and Chen C D 2005 Positioning of extended individual DNA molecules on electrodes by non-uniform AC electric fields *Nanotechnology* 16 2738
- [35] Hai X, Li Y, Yu K, Yue S, Li Y, Song W, Bi S and Zhang X 2021 Synergistic *in-situ* growth of silver nanoparticles with nanozyme activity for dual-mode biosensing and cancer theranostics *Chin. Chem. Lett.* 32 1215–9

- [36] Darjee S M, Bhatt K D, Panchal U S and Jain V K 2017 Scrupulous recognition of biologically important acids by fluorescent "turn off-on" mechanism of thaicalix reduced silver nanoparticles Chin. Chem. Lett. 28 312–8
- [37] Ramos A, García-Sánchez P and Morgan H 2016 AC electrokinetics of conducting microparticles: a review Curr. Opin. Colloid Interface Sci. 24 79–90
- [38] Gierhart B C, Howitt D G, Chen S J, Smith R L and Collins S D 2007 Frequency dependence of gold nanoparticle superassembly by dielectrophoresis *Langmuir* 23 12450–6
- [39] Jackson J D 1999 Classical Electrodynamics (Wiley)
- [40] Shelton W A, Bonin K D and Walker T G 2005 Nonlinear motion of optically torqued nanorods *Phys. Rev.* E 71 036204
- [41] Ahmed W, Kooij E S, Van Silfhout A and Poelsema B 2009 Quantitative analysis of gold nanorod alignment after electric field-assisted deposition *Nano Lett*. 9 3786–94
- [42] Lakowicz J R *et al* 2004 Advances in surface-enhanced fluorescence *J. Fluorescence* **14** 425–41
- [43] Barnes W L 1998 Fluorescence near interfaces: the role of photonic mode density J. Mod. Opt. 45 661–99

- [44] Rai V N, Srivastava A K, Mukherjee C and Deb S K 2012 Surface enhanced absorption and transmission from dye coated gold nanoparticles in thin films *Appl. Opt.* 51 2606–15
- [45] Jain P K, Eustis S and El-Sayed M A 2006 Plasmon coupling in nanorod assemblies: optical absorption, discrete dipole approximation simulation, and exciton-coupling model *J. Phys. Chem.* A 110 18243–53
- [46] Weber W H and Eagen C F 1979 Energy transfer from an excited dye molecule to the surface plasmons of an adjacent metal *Opt. Lett.* 4 236–8
- [47] Tame M S, McEnery K R, Özdemir Ş K, Lee J, Maier S A and Kim M S 2013 Quantum plasmonics *Nat. Phys.* **9** 329–40
- [48] Chance R R, Prock A and Silbey R 1974 Lifetime of an emitting molecule near a partially reflecting surface *J. Chem. Phys.* **60** 2744–8
- [49] Dewarrat F, Calame M and Schönenberger C 2002 Orientation and positioning of DNA molecules with an electric field technique Single Mol. 3 189–93
- [50] Velmanickam L, Jayasooriya V and Nawarathna D 2021 Integrated dielectrophoretic and impedimetric biosensor provides a template for universal biomarker sensing in clinical samples *Electrophoresis* 42 1060–9